

Scalar mesons and low-mass sigma: Does the σ reveal the confinement singularity?

V.V. Anisovich

July 30, 2021

Abstract

I present a short review of the current understanding of the scalar meson sector, with special attention to the problem of the low-mass σ . The dispersion relation N/D -method used for the restoration of the low-energy $\pi\pi$ ($IJ^{PC} = 00^{++}$)-wave amplitude is discussed. The low-energy $\pi\pi$ amplitude was determined from the data in the energy region 280–500 MeV and it was sewn with the previously found K -matrix solution for the region 450–1950 MeV. The N/D -amplitude has a pole on the second sheet of the complex- s plane, near the $\pi\pi$ threshold at $\sqrt{s} \simeq 430 - i325$ MeV, that corresponds to the low-mass σ -meson. I discuss the hypothesis that this pole may be related to the confinement forces, thus being the eyewitness of confinement.

Introduction

In the region of strong interactions, the fundamental objects of QCD, quarks and gluons, may substantially change their characteristics as compared to those at small distances. Phenomenological investigations, as well as theoretical estimates, show that in the strong interaction region we deal with constituent quarks and effective massive gluons (for more detail see, for example, [1] and references therein). In the paper [2], V.N. Gribov drew the attention of the reader to the fact that strong interactions, especially interactions caused by the confinement forces, may form particles which are different from the standard (non-exotic) mesons and baryons. First of all, it concerned the sector of scalar mesons. In the present paper, I discuss the hypothesis of whether the low-mass σ meson, if it exists, may point to the existence of the amplitude singularities related to confinement.

1 Scalar mesons

In this Section, I briefly present the results of the K -matrix analysis for the ($J^P = 0^+$)-wave resonances and the nonet classification of these states. Special attention is paid to the status of $f_0(980)$, $a_0(980)$ and $f_0(1300)$.

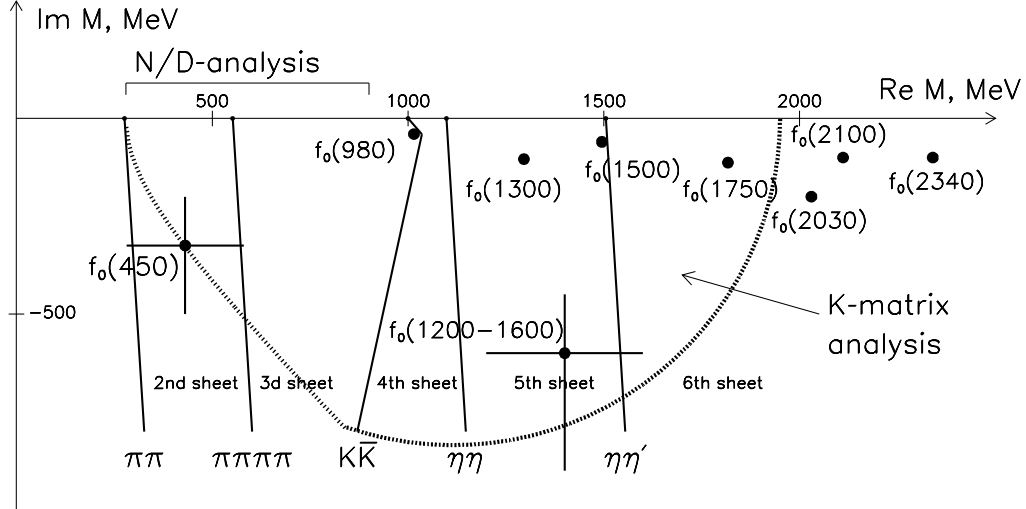


Figure 1: Complex M plane ($M \equiv \sqrt{s}$) in the ($IJ^{PC} = 00^{++}$) sector. Dashed line encircles the part of the plane where the K -matrix analysis reconstructs the analytical K -matrix amplitude: in this area the poles corresponding to the resonances $f_0(980)$, $f_0(1300)$, $f_0(1500)$, $f_0(1750)$ and the broad state $f_0(1200 – 1600)$ are located. On the border of this area the light σ -meson denoted as $f_0(450)$ is shown (the position of the pole corresponds to that found in the N/D method). Beyond the K -matrix analysis area, there are resonances $f_0(2030)$, $f_0(2100)$, $f_0(2340)$.

1.1 K -matrix analysis at $\sqrt{s} > 450$ MeV

The experimental data on meson spectra accumulated by several groups, see [3, 4, 5, 6, 7, 8, 9], provided us with a good basis for the study of the ($IJ^{PC} = 00^{++}$)-wave; the K -matrix analysis of the reactions $\pi\pi \rightarrow \pi\pi$, $K\bar{K}$, $\eta\eta$, $\eta\eta'$, $\pi\pi\pi\pi$ was carried out over the mass range 450–1900 MeV in a set of papers [10, 11, 12]. Also the K -matrix analysis has been performed for the waves 10^+ [11] and $\frac{1}{2}0^+$ [13], thus making it possible to establish the $q\bar{q}$ systematic of scalars for $1^3P_0q\bar{q}$ and $2^3P_0q\bar{q}$ multiplets.

In the scalar-isoscalar sector, $IJ^{PC} = 00^{++}$, the following states are seen:

$$00^{++} : \quad f_0(980), f_0(1300), f_0(1500), \\ f_0(1200 – 1600), f_0(1750). \quad (1)$$

The location of corresponding poles on the complex-mass plane ($\sqrt{s} \equiv M$) is shown in Fig. 1.

The $f_0(980)$ is a well-known resonance, its properties and its nature are intensively discussed during several decades. In the compilation [14], the $f_0(1300)$ is denoted as $f_0(1370)$, however, following the most accurate determination, its mass is near 1300 MeV – so the notation $f_0(1300)$ is used here. The $f_0(1500)$ resonance had been discovered in [15, 16, 17], now it is a well-established state. A few years ago, there existed a strong belief that in the region around 1700 MeV a comparatively narrow state $f_J(1710)$ was present, with $J = 0$ or 2. But the K -matrix analysis

[10, 11, 12] pointed to the resonance $f_0(1750)$, with the width $\Gamma \sim 140 - 300$ MeV: the uncertainty in the definition of its width is due to a poor knowledge of the $\pi\pi\pi\pi$ channel in this mass range and, correspondingly, to the two available solutions, $\Gamma \sim 140$ MeV and $\Gamma \sim 300$ MeV.

The broad state $f_0(1200 - 1600)$, with a half-width 500 – 900 MeV, is definitely needed for the K -matrix analysis. In [11], this state had been denoted as $f_0(1530^{+90}_{-250})$: a large error in the definition of the mass is due to the remoteness of the pole from the real axis (physical region) as well as to the existence of several solutions given by the K -matrix analysis.

The analysis of a large number of reactions, where the broad state $f_0(1200 - 1600)$ reveals itself, proved the validity of the factorisation inherent in the resonance amplitude: near the pole the amplitude is represented as $g_{in}(s - M^2)^{-1}g_{out}$, where the universal coupling constants g_{in} and g_{out} depend on the type of the initial and final states only. A strong production of the $f_0(1200 - 1600)$ in various processes allowed us to fix reliably these coupling constants.

In the 10^{++} , $\frac{1}{2}0^+$ sectors, the K -matrix analysis [11, 13] pointed to the presence of the following resonances:

$$10^{++} : a_0(980), a_0(1520) , \quad (2)$$

$$\frac{1}{2}0^+ : K_0(1415), K_0(1820) . \quad (3)$$

Consideration of the K -matrix bare states argues that the resonances (1) and (2) are related to the first and second $q\bar{q}$ nonets:

$$n = 1 : f_0(980), f_0(1300), a_0(980), K_0(1415) , \quad (4)$$

$$n = 2 : f_0(1500), f_0(1750), a_0(1520), K_0(1820) ,$$

where n is the radial quantum number of the $q\bar{q}$ systems; the broad state $f_0(1200 - 1600)$ is the descendant of the scalar glueball.

1.1.1 The K -matrix bare states

A significant trait of the K -matrix analysis is that it also gives us, along with the characteristics of real resonances, the positions of levels before the onset of the decay channels, i.e. it determines the bare states. In addition, the K -matrix analysis allows one to observe the transformation of bare states into real resonances.

Let us illustrate the determination of bare states in the K -matrix technique using a simple example of the one-channel amplitude (for example, $\pi\pi \rightarrow \pi\pi$) with one-resonance state. The amplitude is written as follows:

$$A(s) = \frac{K(s)}{1 - i\rho(s)K(s)} , \quad (5)$$

where $\rho(s) = \sqrt{1 - 4m_\pi^2/s}$ is the phase space factor and the K -matrix block contains a pole term related to the bare state:

$$K(s) = \frac{g_{bare}^2}{m_{bare}^2 - s} + f. \quad (6)$$

One may re-write (5) to the form

$$A(s) = \frac{g_{bare}^2 + (m_{bare}^2 - s)f}{m_{bare}^2 - s - i\rho(s)[g_{bare}^2 + (m_{bare}^2 - s)f]}, \quad (7)$$

which, near $s = m_{bare}^2$, turns into the standard Breit-Wigner expression:

$$A(s) = \frac{g_{bare}^2}{m_{bare}^2 - s - i\rho(m_{bare}^2)g_{bare}^2}. \quad (8)$$

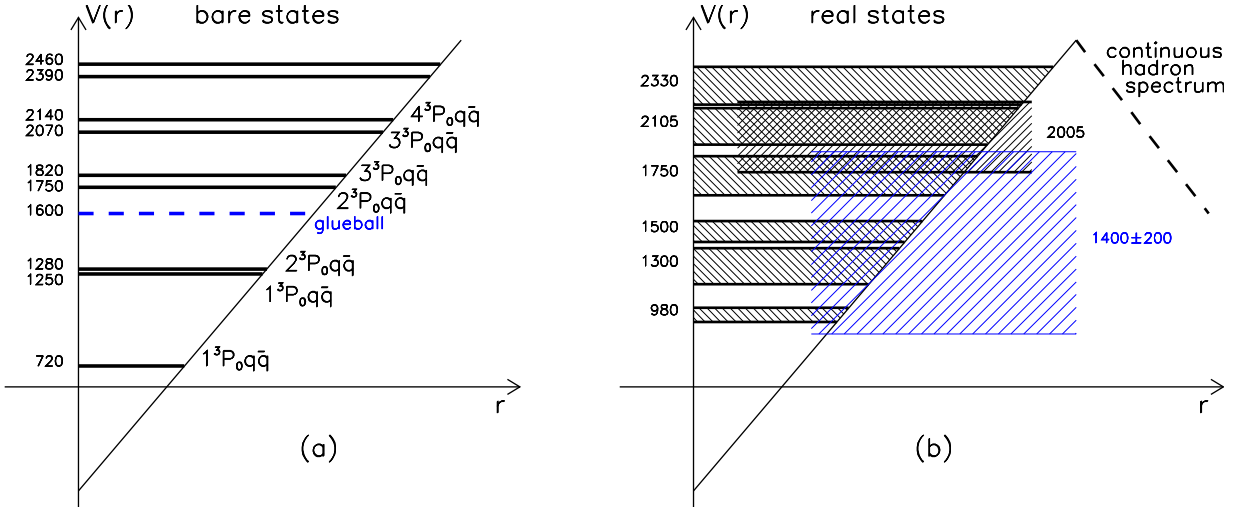


Figure 2: Illustration of the transform of the bare 00^{++} -states into real resonances: a) bare states are the levels in a well with impenetrable wall; b) after the onset of the decay channels (under-barrier transitions), the stable levels transform into real resonances.

If the imaginary part in the denominator in (8) is neglected, one has a pole at $s = m_{bare}^2$ corresponding to the stable level in Fig. 2a, while the pole in (7) describes the unstable state of Fig. 2b.

Considering scalar resonances [10, 11, 12, 13], several coupled channels were analysed, with the inclusion of several resonances into the fitting procedure. This corresponded to the amplitude represented in the matrix form, $\hat{A}(s)$, and the matrix metrics was determined by a number of channels:

$$\hat{A}(s) = \frac{\hat{K}(s)}{1 - i\hat{\rho}(s)\hat{K}(s)}. \quad (9)$$

Here $\hat{\rho}(s)$ is the diagonal phase space matrix; in [10, 11, 12, 13], $\hat{K}(s)$ was parameterised in the following form:

$$K_{ab}(s) = \sum_n \frac{g_{n(bare)}^{(a)} g_{n(bare)}^{(b)}}{m_{n(bare)}^2 - s} + f^{(ab)}(s) . \quad (10)$$

The indices a, b run over different channels, while n refers to the bare states; $f^{(ab)}(s)$ is a smooth background term. The positions of amplitude poles are defined by the equality:

$$\det |1 - i\hat{\rho}(s)\hat{K}(s)| = 0 , \quad (11)$$

which determines masses and widths of resonances, while the masses of bare states are determined by the K -matrix poles (10).

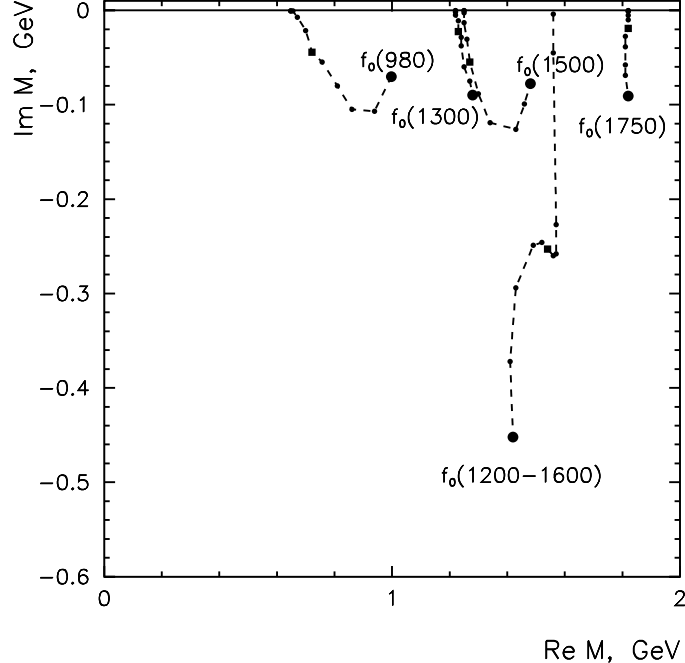


Figure 3: Complex- M plane: trajectories of poles related to the states $f_0(980)$, $f_0(1300)$, $f_0(1500)$, $f_0(1750)$, $f_0(1200 - 1600)$, under a uniform onset of the decay channels.

This evolution of states is illustrated by Fig. 3, where the trajectories of amplitude poles in the complex plane are shown depending on the gradual onset of the decay channels. Technically, it is not difficult to switch on/off the decay channels for the K -matrix amplitude: one should substitute in the K -matrix elements (10):

$$g_{n(bare)}^{(a)} \rightarrow \xi_n(x)g_{n(bare)}^{(a)} , \quad f^{ab} \rightarrow \xi_f(x)f^{ab} , \quad (12)$$

where the parameter-functions for switching on/off the decay channels, $\xi_n(x)$ and $\xi_f(x)$, satisfy the following constraints: $\xi_n(0) = \xi_f(0) = 0$ and $\xi_n(1) = \xi_f(1) = 1$, and x varies in the interval $0 \leq x \leq 1$. Then, at $x = 0$, the amplitude \hat{A} turns into the K -matrix, $\hat{A}(x \rightarrow 0) \rightarrow \hat{K}$, and the amplitude poles occur on the real axis, corresponding to the stable f_0^{bare} -states. At $x = 1$, we deal with the real resonance; varying x from $x = 0$ to $x = 1$ we observe the movement of poles in the complex M -plane.

1.1.2 Quark combinatoric rules for the decay couplings of the quark-antiquark states

The K -matrix amplitude analysis is a good instrument to perform the $q\bar{q}$ nonet classification of mesons in terms of the bare states. The necessity to use bare states but not real resonances is dictated by the fact that decay processes produces a strong mixing of scalar states, for in the transitions $(q\bar{q})_1 \rightarrow \text{real mesons} \rightarrow (q\bar{q})_2$ the orthogonality of the states is not preserved.

The decay couplings of the $q\bar{q}$ -meson or glueball to a pair of mesons are determined by the planar diagrams with $q\bar{q}$ -pairs produced by gluons: these diagrams provide the leading terms in the $1/N$ expansion [18], while nonplanar diagrams give the next-to-leading order contribution. The examples of planar diagrams for the decay of quarkonium and gluonium states are presented in Fig. 4.

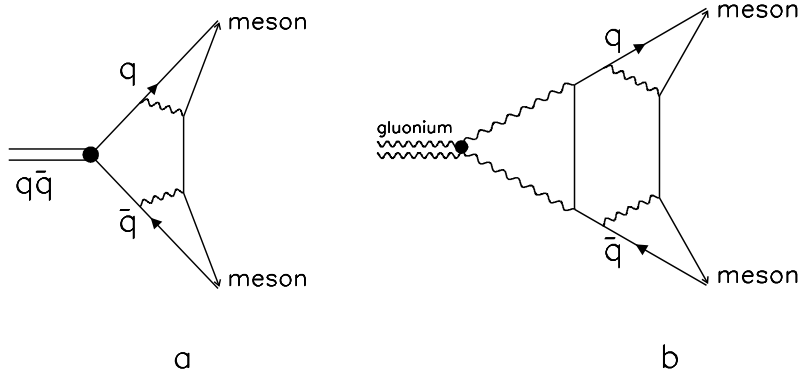


Figure 4: (a,b) Examples of planar diagrams responsible for the decay of the $q\bar{q}$ -state and gluonium into two $q\bar{q}$ -mesons (leading terms in the $1/N$ expansion).

The production of soft $q\bar{q}$ pairs by gluons violates flavour symmetry, with the following ratios of the production probabilities:

$$u\bar{u} : d\bar{d} : s\bar{s} = 1 : 1 : \lambda . \quad (13)$$

The suppression parameter λ for the production of strange quarks varies in the interval $0 \leq \lambda \leq 1$. The estimate made for high energy collisions gives $\lambda = 0.4 - 0.6$ [1], while in hadron decays it was evaluated as $\lambda \simeq 0.8$ [19].

In the K-matrix analysis, the quark combinatorial relations are imposed for the decay couplings of bare states, $g_{n(bare)}^{(a)}$. The quark combinatoric rules were initially suggested for the high energy hadron production [20] and then extended for hadronic J/Ψ decays [21]. The quark combinatoric relations were used for the decay couplings of the scalar–isoscalar states in the analysis of the quark–gluonium content of resonances in [22] and later on in [10, 11, 12, 13].

For the decay couplings of a_0 states, the planar diagrams of the Fig. 4a-type give the following relations:

$$a_0^- \rightarrow K^- K^0 : \frac{g\sqrt{\lambda}}{2} , \quad a_0^- \rightarrow \eta\pi^- : \frac{g\cos\Theta}{\sqrt{2}} , \quad a_0^- \rightarrow \eta'\pi^- : \frac{g\sin\Theta}{\sqrt{2}} . \quad (14)$$

Here g is a universal coupling constant, which is considered in the K-matrix fit as an unknown parameter, and Θ is the mixing angle of the $n\bar{n} = (u\bar{u} + d\bar{d})/\sqrt{2}$ and $s\bar{s}$ components in η and η' : $\eta = n\bar{n}\cos\Theta - s\bar{s}\sin\Theta$ and $\eta' = n\bar{n}\sin\Theta + s\bar{s}\cos\Theta$, the data give us $\Theta \simeq 38^\circ$ [14, 23].

For the decay of scalar K_0 , the couplings are as follows:

$$\begin{aligned} K_0^0 \rightarrow K^+\pi^- &: \frac{g}{2} , \quad K_0^0 \rightarrow K^0\pi^0 : -\frac{g}{2\sqrt{2}} , \\ K_0^0 \rightarrow K^0\eta &: \frac{g}{2} \left(\frac{1}{\sqrt{2}} \cos\Theta - \sqrt{\lambda} \sin\Theta \right) , \\ K_0^0 \rightarrow K^0\eta' &: \frac{g}{2} \left(\frac{1}{\sqrt{2}} \sin\Theta + \sqrt{\lambda} \cos\Theta \right) . \end{aligned} \quad (15)$$

The scalar–isoscalar f_0 -states can be a mixture of the quark–antiquark and gluonium components, $q\bar{q}\cos\alpha + gg\sin\alpha$, where the $q\bar{q}$ -state is the mixture of nonstrange and strange quarks, $n\bar{n} = (u\bar{u} + d\bar{d})/\sqrt{2}$ and $s\bar{s}$:

$$q\bar{q} = n\bar{n}\cos\varphi + s\bar{s}\sin\varphi . \quad (16)$$

For the pure $q\bar{q}$ state, the quark combinatorics gives us the following couplings in the leading terms of the $1/N$ -expansion:

$$\begin{aligned} f_0(q\bar{q}) \rightarrow \pi^+\pi^-, \pi^0\pi^0 &: \frac{g}{\sqrt{2}} \cos\varphi , \\ f_0(q\bar{q}) \rightarrow K^+K^-, K^0\bar{K}^0 &: \frac{g}{2} \left(\sin\varphi + \sqrt{\frac{\lambda}{2}} \cos\varphi \right) , \\ f_0(q\bar{q}) \rightarrow \eta\eta &: g \left(\frac{\cos^2\Theta}{\sqrt{2}} \cos\varphi + \sqrt{\lambda} \sin\varphi \sin^2\Theta \right) , \\ f_0(q\bar{q}) \rightarrow \eta\eta' &: g \sin\Theta \cos\Theta \left(\frac{1}{\sqrt{2}} \cos\varphi - \sqrt{\lambda} \sin\varphi \right) . \end{aligned} \quad (17)$$

The quark combinatorics makes it possible to perform the nonet classification of the $q\bar{q}$ bare states. For the members of the same $q\bar{q}$ nonet ($f_0^{(bare)}(1)$, $f_0^{(bare)}(2)$, $a_0^{(bare)}$, $K_0^{(bare)}$) this means:

(1) The angle difference between isoscalar nonet partners should be 90° :

$$\varphi[f_0^{(bare)}(1)] - \varphi[f_0^{(bare)}(2)] \simeq 90^\circ, \quad (18)$$

that gives us the orthogonality of the flavour wave functions of $f_0^{(bare)}(1)$ and $f_0^{(bare)}(2)$.

(2) Coupling constants g presented in Eqs. (14), (15) and (17) should be roughly equal to each other for all nonet partners:

$$g[f_0^{(bare)}(1)] \simeq g[f_0^{(bare)}(2)] \simeq g[a_0^{(bare)}] \simeq g[K_0^{(bare)}]. \quad (19)$$

The approximate equality in (18), (19) follows from the neglect of the next-to-leading terms in (14), (15), (17).

1.1.3 Quark combinatoric relations for the decay couplings of the gluonium state

For the decay of the pure gluonium state, the planar diagrams of Fig. 4b type give us:

$$\begin{aligned} f_0(\text{gluonium}) \rightarrow \pi^+ \pi^-, \pi^0 \pi^0 &: \quad \frac{G}{\sqrt{2+\lambda}}, \\ f_0(\text{gluonium}) \rightarrow K^+ K^-, K^0 \bar{K}^0 &: \quad G \sqrt{\frac{\lambda}{2+\lambda}}, \\ f_0(\text{gluonium}) \rightarrow \eta \eta &: \quad \frac{G}{\sqrt{2+\lambda}} (\cos^2 \Theta + \lambda \sin^2 \Theta), \\ f_0(\text{gluonium}) \rightarrow \eta \eta' &: \quad G \frac{1-\lambda}{\sqrt{2+\lambda}}. \end{aligned} \quad (20)$$

One may see that the relations between the glueball decay couplings and those for the $q\bar{q}$ state with $\cos \varphi = \sqrt{2/(2+\lambda)}$ coincide. It is due to the fact that the quark–antiquark component in the glueball, due to (13), has the following content [24]:

$$(q\bar{q})_{\text{glueball}} = n\bar{n}\sqrt{\frac{2}{2+\lambda}} + s\bar{s}\sqrt{\frac{\lambda}{2+\lambda}}. \quad (21)$$

The appearance of the quark–antiquark component in the glueball is caused by direct gg – $q\bar{q}$ mixing, which is not suppressed by the $1/N$ -expansion rules [18], as well as the mixing related to the decay processes $gg \rightarrow \text{mesons} \rightarrow gg$. So the glueball is the quarkonium–gluonium composition as follows:

$$gg \cos \gamma + (q\bar{q})_{\text{glueball}} \sin \gamma \quad (22)$$

with $\varphi_{\text{glueball}} = \tan^{-1} \sqrt{\lambda/2} \simeq 26^\circ - 33^\circ$ for $\lambda \simeq 0.50 - 0.85$. Since the ratios of couplings for the transitions $gg \rightarrow \pi\pi, K\bar{K}, \eta\eta, \eta\eta'$ are the same for the quarkonium $(q\bar{q})_{\text{glueball}} \rightarrow \pi\pi, K\bar{K}, \eta\eta, \eta\eta'$, we see that the study of hadronic decays only does not permit to fix the mixing angle γ . However, just this equality of ratios allows one to fix unambiguously the glueball candidates.

1.1.4 Nonet classification of scalar bare states in the K -matrix analysis

The nonet classification of scalar bare states has been carried out in [11, 12, 13], where the mesons were found which are needed to fix two nonets $1^3P_0q\bar{q}$ and $2^3P_0q\bar{q}$. The decay couplings to pseudoscalar mesons for nonet states,

$$\begin{aligned} f_0^{bare}(1), f_0^{bare}(2) &\rightarrow \pi\pi, K\bar{K}, \eta\eta, \eta\eta' , \\ a_0^{bare} &\rightarrow \pi\eta, K\bar{K} , \quad K_0^{bare} \rightarrow \pi K, \eta K , \end{aligned} \quad (23)$$

were determined using for each nonet only two parameters (g and φ , see Eqs. (14), (15) and (17)), while the parameter λ was fixed in the interval $0.50 \leq \lambda \leq 0.85$.

The constraints (14), (15) and (17) imposed on the decay couplings (23) provided us with the opportunity to fix unambiguously the states belonging to the basic nonet:

$$\begin{aligned} 1^3P_0q\bar{q} : \quad f_0^{bare}(700 \pm 100), f_0^{bare}(1220 \pm 40) , \\ a_0^{bare}(960 \pm 30), K_0^{bare}(1220^{+50}_{-150}) . \end{aligned} \quad (24)$$

The mixing angles for $f_0^{bare}(700)$ and $f_0^{bare}(1220)$ satisfy the nonet relation (18):

$$\varphi[f_0^{bare}(700)] = -70^\circ \pm 10^\circ , \quad \varphi[f_0^{bare}(1220)] = 20^\circ \pm 10^\circ . \quad (25)$$

Establishing the second nonet, $2^3P_0q\bar{q}$, is a more complicated task. The K -matrix analysis gives us two scalar-isoscalar bare states at 1200–1650 MeV, $f_0^{bare}(1230 \pm 40)$ and $f_0^{bare}(1580 \pm 40)$, whose decay couplings (23) obey the relations appropriate to the glueball.

Systematics of bare $q\bar{q}$ -states on the (n, M^2) -plane helps us to resolve the dilemma about which one of these states is the glueball. There systematics (discussed in more detail in Section 1.2) definitely tell us that the state $f_0^{bare}(1580 \pm 40)$, which is not on the $q\bar{q}$ -trajectory, is an extra one; so furthermore we accept this state to be the glueball:

$$0^{++} \text{ glueball} : \quad f_0^{bare}(1580 \pm 40) . \quad (26)$$

Let us stress once again that couplings for the transitions $f_0^{bare}(1580 \pm 40) \rightarrow \pi\pi, K\bar{K}, \eta\eta, \eta\eta'$ satisfy glueball decay relations (20).

Having accepted $f_0^{bare}(1580 \pm 40)$ to be the non- $q\bar{q}$ -state, the nonet $2^3P_0q\bar{q}$ is constructed in a unique way:

$$\begin{aligned} 2^3P_0q\bar{q} : \quad f_0^{bare}(1230 \pm 40), f_0^{bare}(1800 \pm 30) , \\ a_0^{bare}(1650 \pm 50), K_0^{bare}(1885^{+50}_{-100}) , \end{aligned} \quad (27)$$

with

$$\varphi[f_0^{bare}(1230)] = 40^\circ \pm 10^\circ , \quad \varphi[f_0^{bare}(1800)] = -60^\circ \pm 10^\circ . \quad (28)$$

After switching on the decay channels, the bare states turn into real resonances. For scalar-isoscalar states we have, after the onset of decays, the transformation as

follows:

$$\begin{aligned}
f_0^{bare}(700 \pm 100) &\rightarrow f_0(980) , \\
f_0^{bare}(1220 \pm 40) &\rightarrow f_0(1300) , \\
f_0^{bare}(1230 \pm 40) &\rightarrow f_0(1500) , \\
f_0^{bare}(1580 \pm 40) &\rightarrow f_0(1200 - 1600) , \\
f_0^{bare}(1800 \pm 40) &\rightarrow f_0(1750) .
\end{aligned} \tag{29}$$

Just this transformation of the bare scalar-isoscalar states into real mesons is shown in Fig. 3.

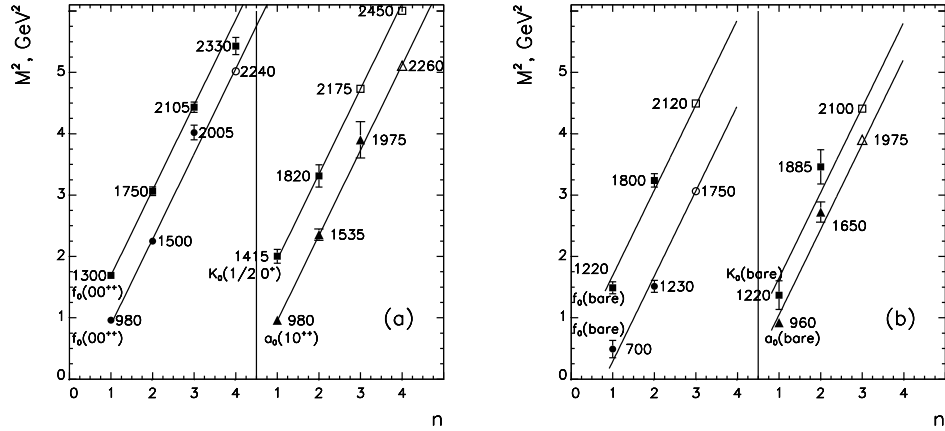


Figure 5: Linear trajectories on the (n, M^2) -plane for scalar resonances (a) and bare scalar states (b). Open circles correspond to the predicted states.

1.2 Systematics of scalar states on the (n, M^2) -plane

The systematics of resonances carried out in [25] demonstrates that all meson resonances can be plotted on linear trajectories in the (n, M^2) -plane, $M^2 = M_0^2 + (n - 1)\mu^2$, with a universal slope $\mu^2 \simeq 1.3 \text{ GeV}^2$.

This empirical property of $q\bar{q}$ states may serve us an additional signature of the $q\bar{q}$ origin of resonances $f_0(980)$, $f_0(1300)$, $f_0(1500)$, $f_0(1750)$. These resonances fit well to linear trajectories, with the slope $\mu^2 \simeq 1.3 \text{ GeV}^2$. Figure 5a demonstrates the (n, M^2) -trajectories for resonance states with 00^{++} , 10^{++} and $\frac{1}{2}0^{++}$, if the $f_0(1200 - 1600)$ is accepted to be the glueball. Note that a doubling of the f_0 -trajectories occurs due to the existence of two components, $n\bar{n}$ and $s\bar{s}$. Similar trajectories for bare states are shown in Fig. 5b, if the $f_0^{bare}(1580)$ is the gluonium. The trajectory slopes for real and bare states almost coincide.

In the variant where $f_0^{bare}(1230)$ is the gluonium, while the $f_0^{bare}(1580)$ is a $q\bar{q}$ state, the linearity of trajectories is completely broken. Correct systematics of the

lowest scalar $q\bar{q}$ states is the basis for a trustworthy search for the glueballs. Precisely these systematics allowed us to identify the broad $f_0(1200 - 1600)$ state as the lowest scalar glueball. Now we have a strong indication for the existence of the tensor glueball [26], thus opening a new page of physics — the glueball physics.

1.3 The $f_0(980)$ and $a_0(980)$: are they the quark-antiquark states?

The nature of mesons $f_0(980)$ and $a_0(980)$ is of principal meaning for the systematics of scalar states and the search for exotic mesons. This is precisely why, till now, there is a lively discussion of the problem of whether the mesons $f_0(980)$ and $a_0(980)$ are the lightest scalar quark-antiquark particles or whether they are exotics, like four-quark ($q\bar{q}q\bar{q}$) states [27], $K\bar{K}$ molecule [28] or minions [29]. An opposite opinion favouring the $q\bar{q}$ structure of $f_0(980)$ and $a_0(980)$ was expressed in [30, 31].

In Sections 1.1 and 1.2, on the basis of the K-matrix analysis and systematisation of scalar mesons on the (n, M^2) -plane, the arguments were discussed favouring the opinion that $f_0(980)$ and $a_0(980)$ are dominantly $q\bar{q}$ states, with a small (10 – 20%) admixture of the $K\bar{K}$ loosely bound component. There exist other arguments, both qualitative and based on the calculation of certain reactions, that also support this idea.

First, let us discuss qualitative arguments.

i) In hadronic reactions, the resonances $f_0(980)$ and $a_0(980)$ are produced as standard, non-exotic resonances, with compatible yields and similar distributions. This phenomenon was observed in the meson central production at high energy hadron–hadron collisions (data of GAMS [32] and Omega [33] collaborations) or hadronic decays of Z^0 mesons (OPAL collaboration [34]).

ii) The exotic nature of $f_0(980)$ and $a_0(980)$ was often argued relying on the surprising proximity of their masses, while it would be natural to expect the variation of masses in the nonet to be of the order of 100–200 MeV. Note that the Breit–Wigner resonance pole, which determines the true mass of the state, is rather sensitive to a small admixture of hadron components, if the production threshold for these hadrons lays nearby. As to $f_0(980)$ and $a_0(980)$, it is easy to see that a small admixture of the $K\bar{K}$ component shifts the pole to the $K\bar{K}$ threshold independently of whether the pole is above or below threshold. Besides, the peak observed in the main mode of the $f_0(980)$ and $a_0(980)$ decays, $f_0(980) \rightarrow \pi\pi$ and $a_0(980) \rightarrow \eta\pi$, is always slightly below the $K\bar{K}$ threshold; this mimics a Breit–Wigner resonance with a mass below 1000 MeV ($K\bar{K}$ threshold). This imitation of a resonance has created the legend about a "surprising proximity" of the $f_0(980)$ and $a_0(980)$ masses.

In fact, the mesons $f_0(980)$ and $a_0(980)$ are characterised not by one pole, as in the Breit–Wigner case, but two poles (see Fig. 6) as in the Flatté formula [35] or K -matrix approach; these poles are rather different for $f_0(980)$ and $a_0(980)$ [11, 12]. Note that the Flatté formula is unable to give us an adequate description of spectra near these poles. So we should apply more complicated representation of the

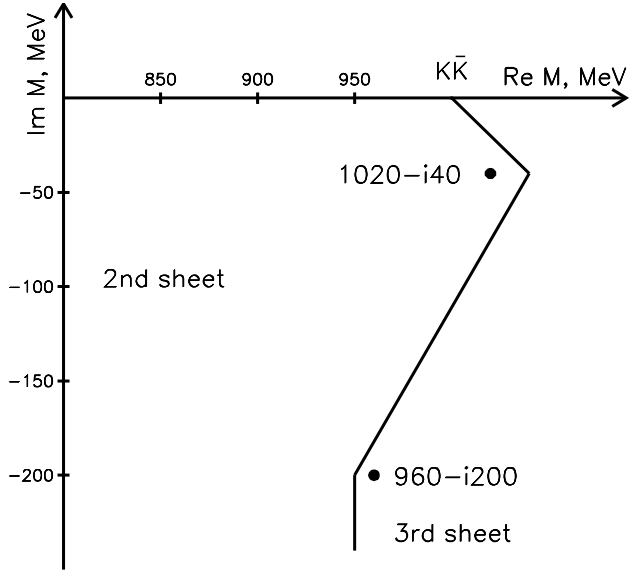


Figure 6: Complex- M plane and location of two poles corresponding to $f_0(980)$; the cut related to the $K\bar{K}$ threshold is shown as a broken line.

amplitude [36, 37] or the K -matrix approach [10, 11, 12], see also [38].

In parallel with the above-mentioned qualitative considerations, there exist convincing arguments which favour the quark-antiquark nature of $f_0(980)$ and $a_0(980)$:

(I) Hadronic decay of the D_s^+ -meson, $D_s^+ \rightarrow \pi^+ f_0(980) \rightarrow \pi^+ \pi^+ \pi^-$: on the quark level, the decay goes as $c\bar{s} \rightarrow \pi^+ s\bar{s} \rightarrow \pi^+ f_0(980)$ thus proving the dominance of the $s\bar{s}$ component in $f_0(980)$. Our analysis [39] showed that $2/3$ $s\bar{s}$ is contained in $f_0(980)$, and this estimate is supported by the experimental value: $BR(\pi^+ f_0(980)) = 57\% \pm 9\%$, and $1/3$ $s\bar{s}$ is dispersed over the resonances $f_0(1300)$, $f_0(1500)$, $f_0(1200 - 1600)$. So the reaction $D_s^+ \rightarrow \pi^+ f_0$ is a measure of the $1^3P_0 s\bar{s}$ component in the f_0 mesons, it definitely tells us about the dominance of the $s\bar{s}$ component in $f_0(980)$, in accordance with results of the K -matrix analysis. The conclusion about dominance of the $s\bar{s}$ component in $f_0(980)$ was also made in the analysis of the decay $D_s^+ \rightarrow \pi^+ \pi^+ \pi^-$ in [40, 41, 42].

(II) Radiative decays $f_0(980) \rightarrow \gamma\gamma$, $a_0(980) \rightarrow \gamma\gamma$ agree well with the calculations [43] based on the assumption of the quark-antiquark nature of these mesons. Let us emphasise again that the calculations favour the $s\bar{s}$ dominance in $f_0(980)$.

(III) Radiative decay $\phi(1020) \rightarrow \gamma f_0(980)$ was a subject of lively discussion in the latest years: there existed an opinion that data on this decay strongly contradict the hypothesis of $q\bar{q}$ nature of $f_0(980)$ [44, 45, 46]. However, our calculations [37, 43] carried out within both relativistic and nonrelativistic approaches showed that the $q\bar{q}$ nature of $f_0(980)$ agrees well with data, see Fig. 7. In [37], we have focused precisely on the applicability of Siegert's theorem [47] to the decay $\phi(1020) \rightarrow \gamma f_0(980)$. We emphasise that $f_0(980)$ is characterized by two poles in the complex-mass plane. Because of that, the notion of mass difference entering Siegert's theorem is not ap-

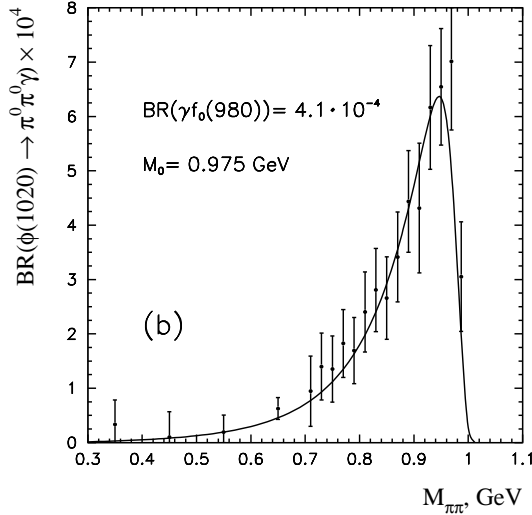


Figure 7: The $\pi\pi$ spectrum from the reaction $\phi(1020) \rightarrow \gamma\pi\pi$ calculated in [35] under the assumption of the $q\bar{q}$ nature of $f_0(980)$. Broad tail on the left (at $M_{\pi\pi} \sim 700-900$ MeV) is due to the contribution of the second pole at $M = 960 - i200$ MeV which is shown in Fig. 6.

plicable to $f_0(700 \pm 100)$. The use of bare states together with K -matrix approach enables us to describe well experimental data, see Fig. 7.

(IV) Convincing argument in favour of the $q\bar{q}$ origin of $a_0(980)$ is given by considering (J, M^2) -planes for isovector states. In Fig. 8, the leading and daughter ρ_J and a_J trajectories are shown. The $a_0(980)$ is located on the first daughter trajectory. Since the ρ_J and a_J trajectories are degenerate, the right-hand side (J, M^2) -plot demonstrates the combined presentation of low-lying trajectories: one can see that the a_0 state is definitely needed near 1000 MeV. Had $a_0(980)$ been considered as exotics and removed from the (J, M^2) -plane, the (J, M^2) -trajectories would definitely demand another a_0 state in this mass region. However, near 1000 MeV we have only one state, $a_0(980)$.

1.4 The $f_0(1300)$: does it exist?

In the compilation [14], the resonance $f_0(1300)$ is denoted as $f_0(1370)$. It was first observed in the combined analysis of the reactions $p\bar{p}$ (at rest, liquid H_2) $\rightarrow \pi^0\pi^0\pi^0$, $\eta\pi^0\pi^0$, $\pi^0\eta\eta$ [15], using also data on $\pi\pi$ -scattering [6]. The following position of the pole was found [15]:

$$M - i\Gamma/2 = (1335 \pm 40) - i(127 + 30/-20) \text{ MeV} . \quad (30)$$

The K-matrix analysis, which included the GAMS [3] and CERN-Münich Collaboration [6] data, gave us [11]:

$$M - i\Gamma/2 = (1300 \pm 20) - i(120 \pm 20) \text{ MeV} . \quad (31)$$

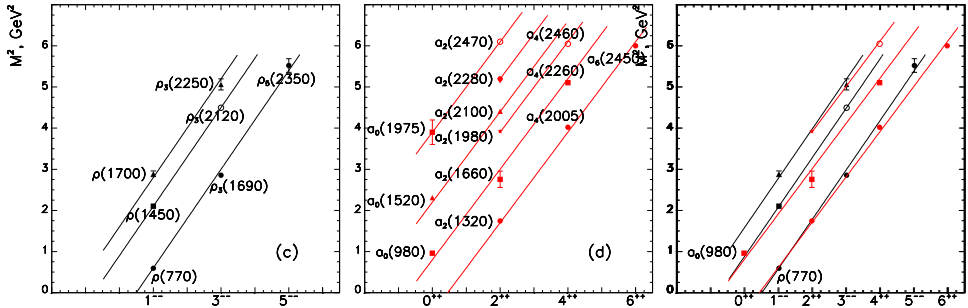


Figure 8: The ρ_J and a_J trajectories on the (J, M^2) -plane; the $a_0(980)$ is on the first daughter trajectory. The right-hand plot is a combined presentation of ρ_J and a_J trajectories: if $a_0(980)$ was not a $q\bar{q}$ state, there should be another a_0 in the mass region ~ 1000 MeV.

The most extensive K-matrix analysis, a combined fit to 16 reactions, led to the following position of the pole [12]:

$$M - i\Gamma/2 = (1315 \pm 20) - i(150 \pm 30) \text{ MeV} . \quad (32)$$

In the reactions $\pi\pi \rightarrow \pi\pi$, $\pi\pi \rightarrow K\bar{K}$, $\pi\pi \rightarrow \eta\eta$, the $f_0(1300)$ is not seen as a peak because of the strong interference with the broad state $f_0(1200 - 1600)$ (or with a "background" in the terminology of papers which work with a narrow mass interval and cannot identify the broad resonance). The $f_0(1300)$ does not reveal itself as a peak in the reactions $p\bar{p} \rightarrow \pi^0\pi^0\pi^0$, $\eta\pi^0\pi^0$, $\pi^0\eta\eta$ as well, but in these processes it is traced on the Argand-plot: with increase of mass, the amplitude creates a circle moving anticlockwise.

The absence of a visible peak corresponding to $f_0(1300)$ in the above-discussed spectra makes some people doubtful about the existence of this resonance. However, let us emphasise that there exist reactions where $f_0(1300)$ is precisely seen as a peak, namely, $\pi^-p \rightarrow \pi^+\pi^-n$, $\pi^0\pi^0n$ at large momentum square transferred to the nucleon $|t| \sim 1 \text{ GeV}^2$ [3, 9], see Figs. 9 and 10.

At $|t| \sim 1 \text{ GeV}^2$, the broad state died, while $f_0(980)$ and $f_0(1300)$ reveal themselves in the $\pi\pi$ spectrum as clear peaks; Figs. 9, 10 show data collected in the interval $0.4 \leq |t| \leq 1.5 \text{ GeV}^2$ (the data [9] cover a wider mass range — here, on the edge of the spectrum, a small peak is seen at $M = 1500$ MeV; it corresponds to $f_0(1500)$). Therefore, the experiments [3, 9] answer the question of whether $f_0(1300)$ is directly seen in the spectra as a peak — yes, it is.

Now let us survey the situation with the determination of parameters of $f_0(1300)$ (or $f_0(1370)$ in the terminology of the PDG [14]).

Determination of resonance parameters with the width about 300 MeV can be done in two ways:

(i) In the reaction, if any, with a small background.

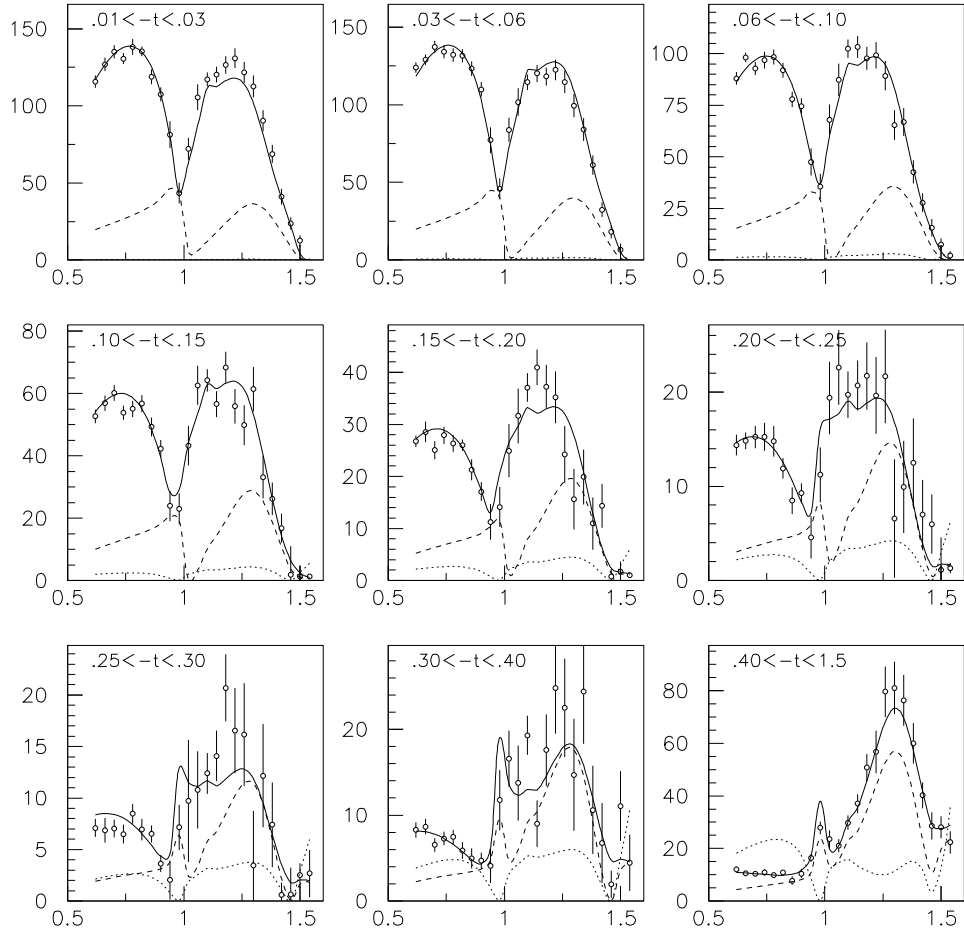


Figure 9: Description of the E852 data in the K-matrix analysis [12] (number of events versus $M_{\pi\pi}$, in GeV) at different t -intervals, in $(\text{GeV}/c)^2$. Dashed curves show contributions from the $a_{1(\text{leading})}$ reggeon trajectory and dotted curves from the $\pi_{(\text{daughter})}$ trajectory; full curves correspond to total three-reggeon contributions: $\pi_{(\text{leading})} + a_{1(\text{leading})} + \pi_{(\text{daughter})}$.

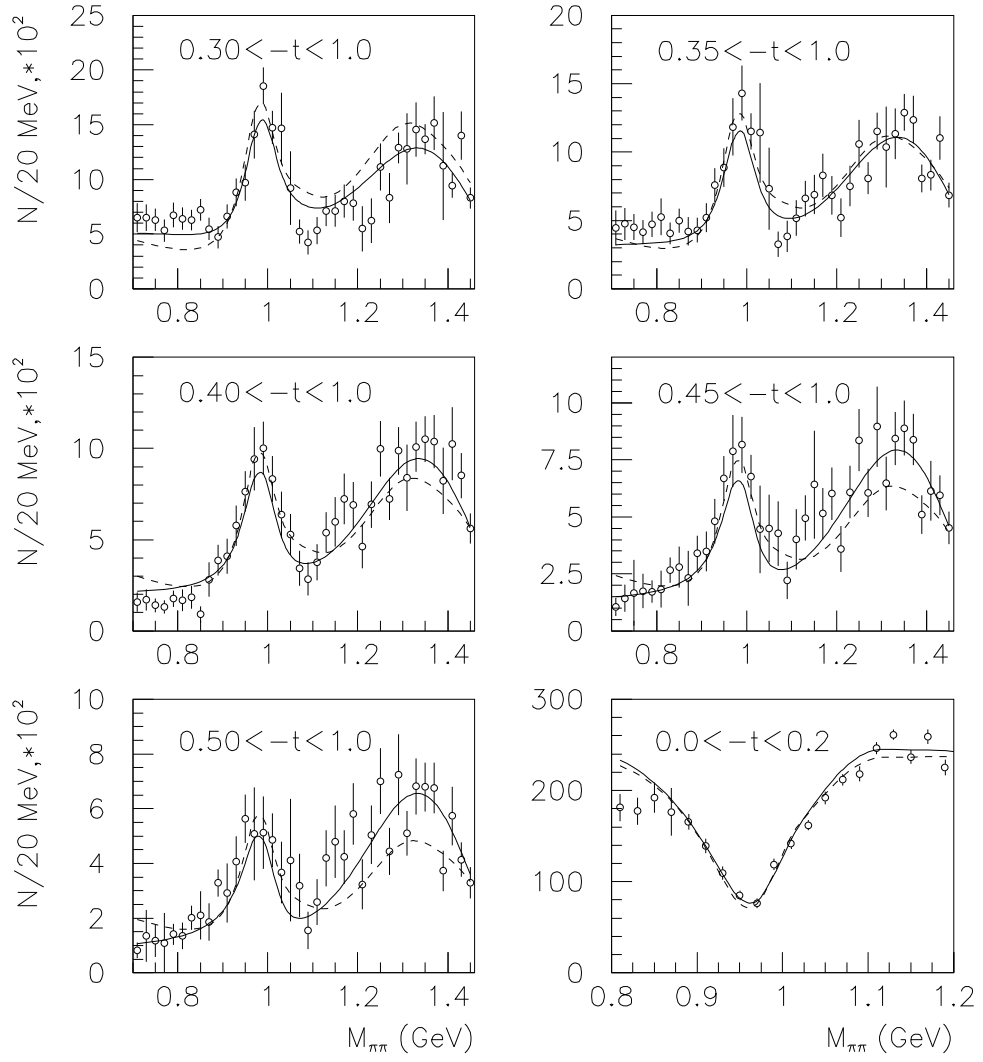


Figure 10: Results of the K-matrix analysis [12]: description of the GAMS data at different t -intervals by taking account of the t -channel reggeon exchanges $\pi_{(leading)}$ + $a_{1(leading)} + \pi_{(daughter)}$ – full curves. Dashed curves refer to the solution found in previous analysis [11].

(ii) But if we deal with a resonance produced in reactions with a considerable background, it is necessary to use as many reactions as possible, so as to determine resonance parameters using the resonance circles on the Argand-plot. The point is that the position of any resonance in the complex M -plane is a universal characteristic, while backgrounds may be different in different processes. So, precisely the use of a large number of channels gives us the way to a reliable determination of universal characteristics.

In [12] the parameters of the $f_0(1300)$ were fixed in both ways: in a background-free production reaction and in reactions with a considerable background — the reaction characteristics emerged as reasonably compatible.

Figures 9 and 10 demonstrate that a resonance, appearing in a reaction with large background, can be seen in the spectrum either as a peak or as a dip, or even as a shoulder, i.e. it can be simply "invisible". In the case, when one–two reactions are studied only, one inevitably gets an error in the mass definition, of the order of $\Gamma/2$. This is a systematic error; it depends on the method of fitting and on the background parameterisation. Concerning the PDG-compilation, we may conclude that precisely such definitions of mass and width of $f_0(1370)$ have been collected there. Of course, such a heap of numbers cannot be trusted. Also it is worth mentioning that averaging over systematic errors is not a correct procedure.

2 The σ -meson

In this Section, a dispersion relation is used to reconstruct the $\pi\pi$ scattering amplitude in the region of small $M_{\pi\pi}$; it is then sewn with the K -matrix solution given in [10, 11, 12] for $M_{\pi\pi} \sim 450 - 1950$ MeV. The procedure is as follows. Data for δ_0^0 are used to construct the N/D amplitude below 900 MeV; the result is then sewn together with the K -matrix amplitude, with the purpose of making a continuation to the region $s = M_{\pi\pi}^2 \sim 0$. In this procedure, we strictly follow the results obtained for the K -matrix amplitude in the region 450–900 MeV, where we may be confident of the results of the K -matrix representation. Recall that the K -matrix representation allows us to reconstruct correctly the analytical structure of the amplitude in the region $s > 0$ (threshold and pole singularities) but not the left-hand side singularities at $s \leq 0$ (singularities related to forces). Therefore, being cautious, we cannot be quite sure about the validity of K -matrix results below the $\pi\pi$ threshold.

The dispersion relation amplitude is found here using the method suggested in [48, 49]. The constructed N/D -amplitude provides a good description of δ_0^0 from threshold to 900 MeV, thus including the region $\delta_0^0 \sim 90^\circ$. This amplitude does not have a pole at 500–900 MeV; instead, the pole is located near the $\pi\pi$ threshold.

I discuss the hypothesis that the low-mass pole in the scalar–isoscalar wave is related to a fundamental phenomenon at large distances (in hadronic scale). I argue that the low-mass pole corresponds to a white composite particle which is inherent in subprocesses responsible for colour confinement forces.

2.1 Dispersion relation solution for the $\pi\pi$ -scattering amplitude below 900 MeV

The pion–pion partial scattering amplitude is a function of the invariant energy squared, $s = M_{\pi\pi}^2$. It can be represented as a ratio $N(s)/D(s)$, where $N(s)$ has a left-hand cut, due to "forces" (interactions owing to t - and u -channel exchanges); the function $D(s)$ is determined by the rescattering in the s -channel. $D(s)$ is given by the dispersion integral along the right-hand cut in the complex- s plane:

$$A(s) = \frac{N(s)}{D(s)}, \quad D(s) = 1 - \int_{4\mu_\pi^2}^{\infty} \frac{ds'}{\pi} \frac{\rho(s')N(s')}{s' - s + i0}. \quad (33)$$

Here $\rho(s)$ is the invariant $\pi\pi$ phase space, determined as $\rho(s) = (16\pi)^{-1} \sqrt{1 - 4\mu_\pi^2/s}$. It was supposed in (33) that $D(s) \rightarrow 1$ as $s \rightarrow \infty$ and CDD-poles are absent; (a detailed description of the N/D -method may be found in [51]).

The N -function can be written as an integral along the left-hand cut as follows:

$$N(s) = \int_{-\infty}^{s_L} \frac{ds'}{\pi} \frac{L(s')}{s' - s}, \quad (34)$$

where the value s_L marks the beginning of the left-hand cut. For example, for the one-meson exchange diagram $g^2/(m^2 - t)$, the left-hand cut starts at $s_L = 4\mu_\pi^2 - m^2$, and the N -function at this point has a logarithmic singularity; for the two-pion exchange, $s_L = 0$.

Below we work with the amplitude $a(s)$, which is defined as follows:

$$a(s) = \frac{N(s)}{8\pi\sqrt{s} \left(1 - P \int_{4\mu_\pi^2}^{\infty} \frac{ds'}{\pi} \frac{\rho(s')N(s')}{s' - s} \right)}. \quad (35)$$

The amplitude $a(s)$ is related to the scattering phase shift: $a(s)\sqrt{s/4 - \mu_\pi^2} = \tan\delta_0^0$. In (35), the threshold singularity is explicitly singled out, so the function $a(s)$ contains the obly the left-hand cut plus poles corresponding to zeros of the denominator of the right-hand side (35): $1 = P \int_{4\mu_\pi^2}^{\infty} (ds'/\pi) \cdot \rho(s')N(s')/(s' - s)$. The pole of $a(s)$ at $s > 4\mu_\pi^2$ corresponds to the phase shift value $\delta_0^0 = 90^\circ$. The phase of the $\pi\pi$ scattering reaches the value $\delta_0^0 = 90^\circ$ at $\sqrt{s} = M_{90} \simeq 850$ MeV. Because of that, the amplitude $a(s)$ may be represented in the form:

$$a(s) = \int_{-\infty}^{s_L} \frac{ds'}{\pi} \frac{\alpha(s')}{s' - s} + \frac{C}{s - M_{90}^2} + D. \quad (36)$$

For the reconstruction of the low-mass amplitude, the parameters D, C, M_{90} and $\alpha(s)$ have been determined by fitting to experimental data. In the fit we have used a

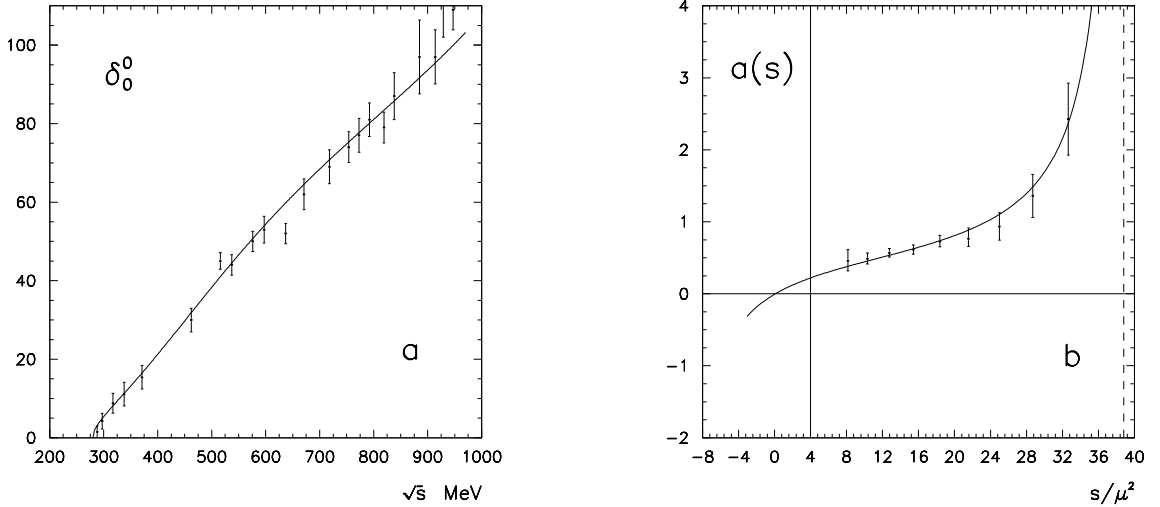


Figure 11: a) Fitting to data on δ_0^0 using the N/D -amplitude. b) Amplitude $a(s)$ in the N/D -solution (solid curve) and the K -matrix approach [4,6] (points with error bars).

method which has been verified in the analysis of low-energy nucleon-nucleon amplitudes [48]. Namely, the integral on the right-hand side of (36) has been substituted by the sum

$$\int_{-\infty}^{s_L} \frac{ds'}{\pi} \frac{\alpha(s')}{s' - s} \rightarrow \sum_n \frac{\alpha_n}{s_n - s} , \quad (37)$$

with $-\infty < s_n \leq s_L$.

The description of data using the N/D -solution with six terms in the sum (37) is demonstrated in Fig. 11a. The parameters entering the amplitude $a(s)$ are given below:

$s_n \mu_\pi^{-2}$	-9.56	-10.16	-10.76	-32	-36	-40
$\alpha_n \mu_\pi^{-1}$	2.21	2.21	2.21	0.246	0.246	0.246
$M_{90} = 6.228 \mu_\pi, \quad C = -13.64 \mu_\pi, \quad D = 0.316 \mu_\pi^{-1}$						

(38)

The scattering length and Adler zero in this solution are equal to

$$a_0^0 \simeq 0.22 \mu_\pi^{-1} \quad s = 0.12 \mu_\pi^2 . \quad (39)$$

The N/D -amplitude is sewn with the K -matrix amplitude of [11, 12], and Fig. 11b demonstrates the level of the coincidence of the amplitudes $a(s)$ for both solutions; (the values of $a(s)$ which correspond to the K -matrix amplitude are shown with error bars determined in [11, 12]).

The dispersion relation solution has a correct analytical structure at $|s| < 1$ GeV 2 . The amplitude has no poles on the first sheet of the complex- s plane; the left-hand cut of the N -function after the substitution (37) transforms into a set of

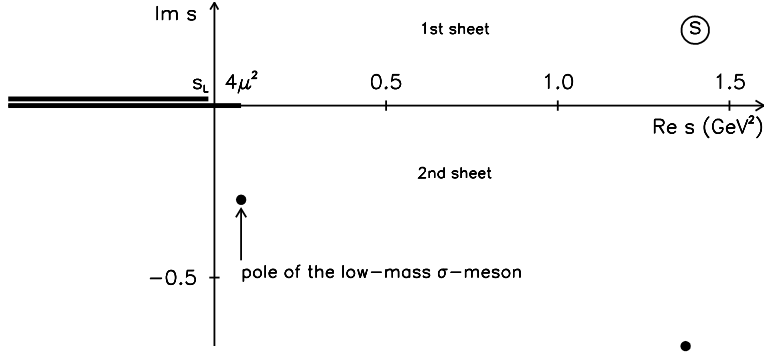


Figure 12: Complex-s plane and singularities of the N/D -amplitude

poles on the negative piece of the real s -axis: six poles of the amplitude (at $s/\mu_\pi^2 = -5.2, -9.6, -10.4, -31.6, -36.0, -40.0$) represent the left-hand singularity of $N(s)$. On the second sheet (under the $\pi\pi$ -cut) the amplitude has two poles: at $s \simeq (4 - i14)\mu_\pi^2$ and $s \simeq (70 - i34)\mu_\pi^2$ (see Fig. 12). The second pole, $s = (70 - i34)\mu_\pi^2$, is located beyond the region under consideration, $|s| < 1 \text{ GeV}^2$; (nevertheless, let us emphasise that the K -matrix amplitude [11, 12] has a pole corresponding to the broad state $f(1200 - 1600)$ just in the region of the second pole of the N/D -amplitude). The pole near the threshold, at

$$s \simeq (4 - i14)\mu_\pi^2, \quad (40)$$

is precisely what we discuss. The N/D -amplitude has no poles at $\text{Re}\sqrt{s} \sim 600 - 900$ MeV, despite the phase shift δ_0^0 reaches 90° here.

The data for δ_0^0 above the $\pi\pi$ threshold do not fix the N/D -amplitude rigidly. The position of the low-mass pole can be easily varied in the region $\text{Re } s \sim (0 - 4)\mu_\pi^2$, and there are simultaneous variations of the scattering length in the interval $a_0^0 \sim (0.21 - 0.28)\mu_\mu^{-1}$ and Adler zero at $s \sim (0 - 1)\mu_\pi^2$. The discussed solution (37) is chosen because recent data for the scattering length $a_0^0 \sim (0.228 \pm 0.015)\mu_\mu^{-1}$ [53] coincide with the value presented in (39).

Let us note that the way of reconstruction of the dispersion relation amplitude used here differs from the mainstream attempts to determine the N/D -amplitude. In the classic N/D procedure, that is the bootstrap one; the pion-pion amplitude is to be determined by analyticity, unitarity and crossing symmetry, giving a unique determination of the left-hand cut by crossing channels. However, the bootstrap procedure was not realised till now; the problems faced by the present bootstrap

program are discussed in [52] and references therein. Nevertheless, one can try to saturate the left-hand cut by known resonances in the crossed channels. Usually it was supposed that dominant contributions to the left-hand cut come from the ρ -meson, $f_2(1275)$ and σ exchanges. Within this scheme, the low-energy amplitude is restored, being corrected by the available experimental data.

In the scheme used here, see also [49], the amplitude in the physical region at 450–1950 MeV is supposed to be known (the result of the K-matrix analysis) – then a continuation of the amplitude is carried out from the region 450–900 MeV to smaller masses; this continuation is corrected by the data. As a result, we reconstruct the pole near the threshold (the low-mass σ -meson) and the left-hand cut (although with lesser accuracy — on a qualitative level).

In approaches which take into account the left-hand cut as a contribution of known meson exchanges, the following low-mass pole positions were obtained:

- (i) dispersion relation approach, $s \simeq (0.2 - i22.5)\mu_\pi^2$ [54],
- (ii) meson exchange models, $s \simeq (3.0 - i17.8)\mu_\pi^2$ [55], $s \simeq (0.5 - i13.2)\mu_\pi^2$ [56],
 $s \simeq (2.9 - i11.8)\mu_\pi^2$ [57].

2.2 Low-mass pole as eyewitness of confinement

It was suggested in [49, 50] that the existence of the light σ -meson may be due to a singular behaviour of forces between quark and antiquark at large distances; (in quark models they are conventionally called "confinement forces"). The scalar confinement potential, which is needed for the description of the spectrum of the $q\bar{q}$ -states in the region 1000–2000 MeV, behaves at large hadronic distances as $V_{\text{confinement}}^{(c)}(r) \sim \alpha r$, where $\alpha \simeq 0.19 \text{ GeV}^2$. In the momentum representation, such a growth of the potential is associated with singular behaviour at small q :

$$V_{\text{confinement}}^{(c)}(q) \sim \frac{1}{q^4}. \quad (41)$$

In colour space, the main contribution comes from the component $c = 8$, i.e. the confinement forces should be the octet ones. The question that is crucial for the structure of the σ -meson is as follows: is there a component with the colour singlet $V_{\text{confinement}}^{(1)}(q)$ in the singular potential (41)?

If the singular component with $c = 1$ exists, then it must reveal itself in hadronic channels as well; that is, in the $\pi\pi$ -channel. In hadronic channels, this singularity should not be exactly the same as in the colour octet ones, because the hadronic unitarization of the amplitude (which is absent in the channel with $c = 8$) should modify somehow the low-energy amplitude. One may believe that, as a result of the unitarization in the channel $c = 1$, i.e. due to the account of hadronic rescattering, the singularity of $V_{\text{confinement}}^{(1)}(q)$ may appear in the $\pi\pi$ -amplitude on the second sheet, being split into several poles. The modelling of the scalar confinement potential, with the account for the decay of unstable levels [58], confirms the pole splitting. One may believe that this singularity is what we call "the light σ -meson".

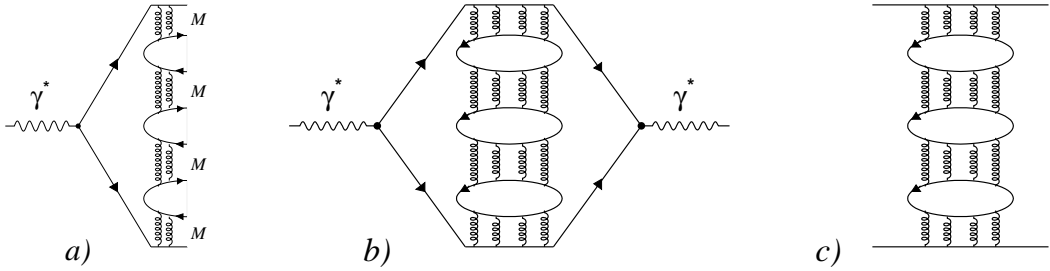


Figure 13: a) Quark–gluonic comb produced by breaking a string by quarks flowing out in the process $e^+e^- \rightarrow \gamma^* \rightarrow q\bar{q} \rightarrow \text{mesons}$. b) Convolution of the quark–gluonic combs. c) Example of diagrams describing interaction forces in the $q\bar{q}$ systems.

Therefore, the main question consists in the following: does the $V_{\text{confinement}}^{(1)}(q^2)$ have the same singular behaviour as $V_{\text{confinement}}^{(8)}(q^2)$? The observed linearity of the (n, M^2) -trajectories, up to the large-mass region, $M \sim 2000 - 2500$ MeV [25], favours the idea of the universality in the behaviour of potentials $V_{\text{confinement}}^{(1)}$ and $V_{\text{confinement}}^{(8)}$ at large r , or small q . To see that (for example, in the process $\gamma^* \rightarrow q\bar{q}$, Fig. 13a) let us discuss the colour neutralisation mechanism of outgoing quarks as a breaking of the gluonic string by newly born $q\bar{q}$ -pairs. At large distances, which correspond to the formation of states with large masses, several new $q\bar{q}$ -pairs should be formed. It is natural to suggest that a convolution of the quark–gluon combs governs the interaction forces of quarks at large distances, see Fig. 13b. The mechanism of the formation of new $q\bar{q}$ -pairs to neutralise colour charges does not have a selected colour component. In this case, all colour components $3 \otimes \bar{3} = 1 + 8$ behave similarly, that is, at small q^2 the singlet and octet components of the potential are uniformly singular, $V_{\text{confinement}}^{(1)}(q^2) \sim V_{\text{confinement}}^{(8)}(q^2) \sim 1/q^4$. This is seen in Fig. 13a. The quark–gluon ladder ensures the t -channel flow of colour charge $c = 3$; so a quark–antiquark interaction amplitude is the convolution of ladder diagrams $3 \otimes \bar{3} = 1 + 8$ and contains two equivalent singlet and octet components. This points to a similarity of $V_{\text{confinement}}^{(1)}$ and $V_{\text{confinement}}^{(8)}$.

3 Conclusion

At the present time, one cannot definitely state that lightest σ meson exists. The K -matrix analysis of meson spectra [12] did not require the introduction of σ meson as an amplitude pole located near the physical region, though its existence was not denied. Analytic continuation of the $\pi\pi \rightarrow \pi\pi$ amplitude from the physical region to $s < 4m_\pi^2$ region, using dispersion N/D methods, points to the existence of a pole near the $\pi\pi$ threshold. However, such an analytic continuation cannot be a convincing argument, because of ambiguities related to the necessity of accounting for the left-hand cut too. The study within the bootstrap procedure, with a reconstruction of the

left-hand cut contribution at $0 \leq |s| \leq 1 \text{ GeV}^2$, could argue for the existence of the light σ meson; however, one needs to make a sewing with the domain of the reggeon approach to the amplitude — such a procedure is still waiting for its realisation.

In case of the existence of the $\pi\pi$ amplitude singularity near $s \sim 4m_\pi^2$, one may think that it is due to "confinement forces". This singularity can be of the pole type or have a more complicated structure. It may be of the type of singularity formed by gluon fields as is shown in Fig. 13b; the inclusion of the quark loops into gluon planar diagrams is rather natural in the N/D expansion rule — they do not lead to additional suppression.

The lightest pseudoscalar and scalar $q\bar{q}$ states are the pairs of the 0^{-+} and 0^{++} mesons as follows: $\eta(550)$, $\eta'(958)$ and $f_0^{bare}(700 \pm 100)$, $f_0^{bare}(1220 \pm 40)$. In both cases the lightest particle ($\eta(550)$ for 0^{-+} and $f_0^{bare}(700 \pm 100)$ for 0^{++}) is close to a flavour octet; that is their common feature. The $f_0^{bare}(700 \pm 100)$ has undergone a noticeable shift of mass in transforming from the bare state to a real meson; that is due to the decay transitions $f_0 \rightarrow \text{real mesons} \rightarrow f_0$ and the proximity of the broad scalar glueball $f_0(1200 - 1600)$ (or maybe the proximity of the σ meson). As a result, we observe the transformation $f_0^{bare}(700 \pm 100) \rightarrow f_0(980)$.

The role of gluonic states in the formation of lowest 0^{-+} mesons is not clear. According to [23], the admixture of gluonium component in the η meson is small, $\leq 5\%$, while in the η' meson it is noticeably larger, $\leq 15\%$. There is a variety of opinions concerning the mass of the pseudoscalar glueball: it is ~ 2400 MeV in lattice calculations [59], or ~ 1500 MeV in string model estimates [60], or ≥ 1700 MeV, as is obtained from the data on J/ψ radiative decay, see [61] and references therein. Therefore, it is rather difficult to say what does it meant by the similarity of flavour structures in $\eta(550)$ and $f_0^{bare}(700 \pm 100)$ (both are nearly flavour octets).

Acknowledgement

I thank A.V. Anisovich, Ya.I. Azimov, D.V. Bugg, L.G. Dakhno, V.A. Nikonov, J. Nyiri, H.R. Petry, A.V. Sarantsev and V.V. Vereshagin for fruitful discussions. The article is supported by the RFBR grant N 04-02-17091.

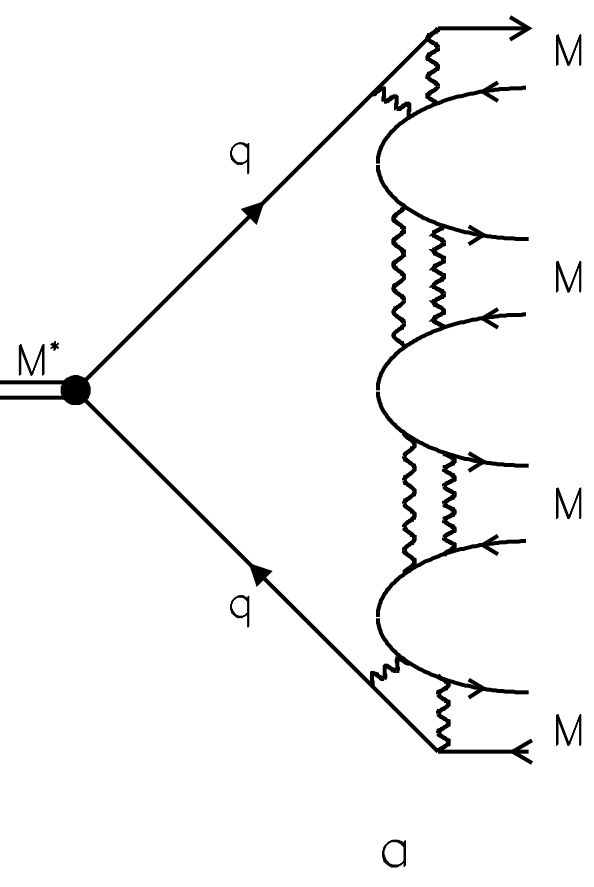
References

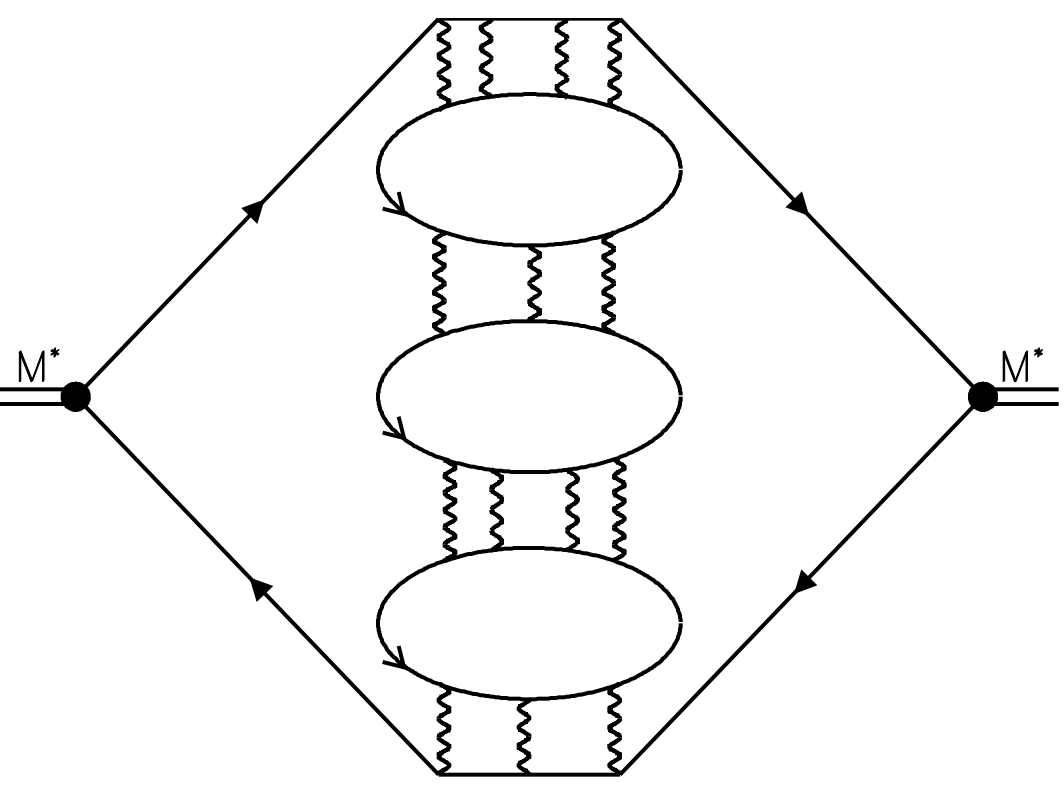
- [1] V.V. Anisovich, J. Nyiri, M.N. Kobrinsky, Yu.M. Shabelski, "Quark Model and High Energy Collisions", 2nd edition, World Scientific, Singapore, 2004.
- [2] V.N. Gribov, Preprint LU-TP 91-7, Lund University, 1991.
- [3] D. Alde *et al.*, *Zeit.Phys. C* **66**, 375 (1995);
Yu.D. Prokoshkin *et al.*, *Physics – Doklady* **342**, 473 (1995);
A.A. Kondashov *et al.*, Preprint IHEP 95-137, Protvino, 1995.

- [4] F. Binon *et al.*, Nuovo Cim. A **78**, 313 (1983); **80**, 363 (1984).
- [5] S.J. Lindenbaum and R.S. Longacre, Phys. Lett. B **274**, 492 (1992);
A. Etkin *et al.*, Phys. Rev. D **25**, 1786 (1982).
- [6] G. Grayer *et al.*, Nucl. Phys. B **74**, 189 (1974);
W. Ochs, PhD Thesis, Münich University (1974).
- [7] C. Amsler *et al.*, Phys. Lett. B **342**, 433 (1995); B **355**, 425 (1995).
- [8] A. Abele *et al.*, Phys. Rev. D **57**, 3860 (1998); Phys. Lett. B **391**, 191 (1997);
B **411**, 354 (1997); B **450**, 275 (1999); B **468**, 178 (1999); B **469**, 269 (1999);
K. Wittmack, PhD Thesis, Bonn University, (2001);
E. Klempt and A.V. Sarantsev, private communication.
- [9] J. Gunter *et al.* (E852 Collaboration), Phys. Rev. D **64**, 007003 (2001).
- [10] V. V. Anisovich, Yu. D. Prokoshkin and A. V. Sarantsev, Phys. Lett. **B389**, 388 (1996).
- [11] V.V. Anisovich, A.A. Kondashov, Yu.D. Prokoshkin, S.A. Sadovsky,
A.V. Sarantsev, Yad. Fiz. **60**, 1489 (2000) [Physics of Atomic Nuclei
60, 1410 (2000)].
- [12] V.V. Anisovich, A.V. Sarantsev, Eur. Phys. J. **A16**, 229 (2003).
- [13] A.V. Anisovich and A.V. Sarantsev, Phys. Lett. B **413**, 137 (1997).
- [14] S. Eidelman *et al.* (PDG), Phys. Lett. B **592**, 1 (2004).
- [15] V.V. Anisovich, D.V. Bugg, A.V. Sarantsev, B.S. Zou, Yad. Fiz. **57**, 1666 (1994)
[Phys. Atom. Nucl. **57**, 1595 (1994)].
- [16] V.V. Anisovich, D.S. Armstrong, I. Augustin, *et al.*, Phys. Lett. B **323**, 233 (1994).
- [17] V.V. Anisovich, D.V. Bugg, A.V. Sarantsev, B.S. Zou, Phys. Rev. D **50**, 1972 (1994).
- [18] G. t'Hooft, Nucl. Phys. B **72**, 461 (1974);
G. Veneziano, Nucl. Phys. B **117**, 519 (1976).
- [19] K. Peters and E. Klempt, Phys. Lett. B **352**, 467 (1995).
- [20] V.V. Anisovich and V.M. Shekhter, Nucl. Phys. B **55**, 455 (1973);
J.D. Bjorken and G.E. Farrar, Phys. Rev. D **9**, 1449 (1974).
- [21] M.A. Voloshin, Yu.P. Nikitin, and P.I. Porfirov, Yad. Fiz. **35**, 1006 (1982) [Sov.
J. Nucl. Phys. **35**, 586 (1982)].

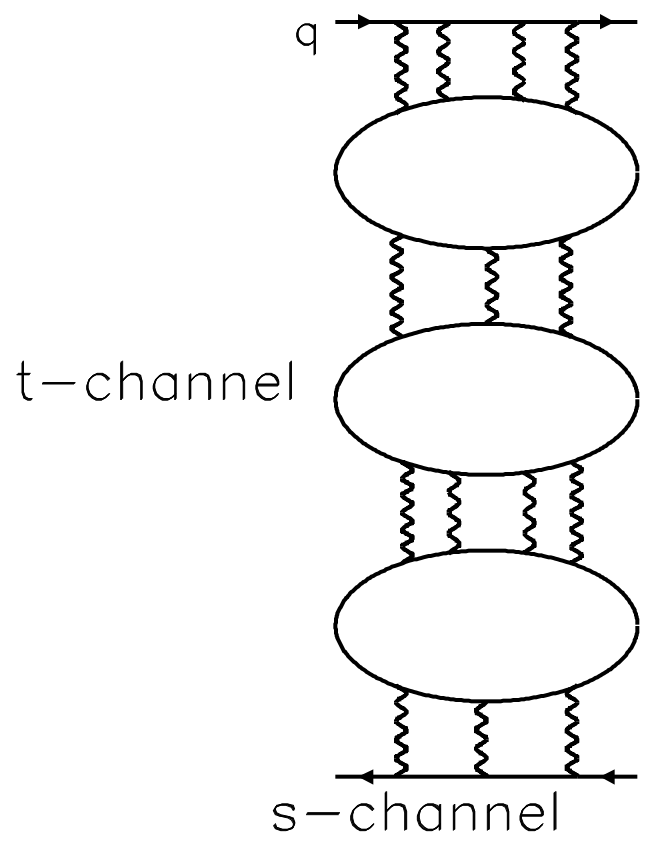
- [22] S.S. Gershtein, A.K. Likhoded, Yu.D. Prokoshkin, *Zeit. Phys. C* **24**, 305 (1984); C. Amsler and F.E. Close, *Phys. Rev. D* **53**, 295 (1996); *Phys. Lett. B* **353**, 385 (1995);
V.V. Anisovich, *Phys. Lett. B* **364**, 195 (1995).
- [23] V.V. Anisovich, D.V. Bugg, V.N. Nikonov, and D.I. Melikhov, *Phys. Lett. B* **404**, 166 (1997).
- [24] A.V. Anisovich, hep-ph/0104005.
- [25] A.V. Anisovich, V.V. Anisovich, and A.V. Sarantsev, *Phys. Rev. D* **62**, 051502(R) (2000).
- [26] V.V. Anisovich, Pis'ma v ZhETF **80**, 845 (2004) [JETP Letters **80**, 715 (2004)];
V.V. Anisovich, A.V. Sarantsev, Pis'ma v ZhETF, **81**, 531 (2005) [JETP Letters **81**, 417 (2005)].
- [27] R. Jaffe, *Phys. Rev. D* **15**, 267 (1977).
- [28] J. Weinstein and N. Isgur, *Phys. Rev. D* **41**, 2236 (1990).
- [29] F.E. Close et al., *Phys. Lett. B* **319**, 291 (1993).
- [30] S. Narison, *Nucl. Phys. B* **509**, 312 (1998); *Nucl. Phys. (Proc. Suppl.)* **B64**, 210 (1998).
- [31] P. Minkowski and W. Ochs, *Eur. Phys. J. C* **9**, 283 (1999).
- [32] D.M. Alde et al., *Phys. Lett. B* **397**, 350 (1997).
- [33] D. Barberis et al., *Phys. Lett. B* **453**, 305 (1999); *Phys. Lett. B* **453**, 325 (1999);
Phys. Lett. B **462**, 462 (1997).
- [34] K. Ackerstaff et al., (OPAL Collab.) *Eur. Phys. J. C* **4**, 19 (1998).
- [35] S.M. Flatté, *Phys. Lett. B* **63**, 224 (1976).
- [36] V.V. Anisovich, V.A. Nikonov, V.A. Sarantsev, *Yad. Fiz.* **65**, 1583 (2002) [*Phys. Atom. Nucl.* **65**, 1545 (2002)]; *Yad. Fiz.* **66**, 772 (2003) [*Phys. Atom. Nucl.* **66**, 741 (2003)].
- [37] A.V. Anisovich, V.V. Anisovich, V.N. Markov, V.A. Nikonov, A.V. Sarantsev, *Yad. Fiz.* in press; hep-ph/0403123.
- [38] K.L. Au, D. Morgan, M.R. Pennington, *Phys. Rev. D* **35**, 1633 (1987); D. Morgan and M.R. Pennington, *Phys. Rev. D* **48**, 1185 (1993).
- [39] V.V. Anisovich, L.G. Dakhno, V.A. Nikonov, *Yad. Fiz.* **67**, 1593 (2004) [*Phys. Atom. Nucl.* **67**, 1571 (2004)].

- [40] A. Deandrea, R. Gatto, G. Nardulli et al., Phys. Lett. B **502**, 79 (2001).
- [41] F. Kleefeld, E. van Beveren, G. Rupp, M.D. Scadron, Phys. Rev. D **66**, 034007 (2002).
- [42] P. Minkowski, W. Ochs, hep-ph/02092223.
- [43] A.V. Anisovich, V.V. Anisovich, V.A. Nikonov, Eur. Phys. J. A **12**, 103 (2001); A.V. Anisovich, V.V. Anisovich, V.N. Markov, V.A. Nikonov, Yad. Fiz. **65**, 523 (2002) [Phys. Atom. Nucl. **65**, 497 (2002)].
- [44] N.N. Achasov, AIP Conf. Proc. **619**, 112 (2002).
- [45] F.E. Close, Int. Mod. Phys. A **17**, 3239 (2002).
- [46] M.A. DeWitt, H.M. Choi, C.R. Ji, Phys. Rev. D **68**, 054026 (2003).
- [47] A.J.F. Siegert, Phys. Rev. **52**, 787 (1937).
- [48] V.V. Anisovich, M.N. Kobrinsky, D.I. Melikhov and A.V. Sarantsev, Nucl. Phys. **A544** (1992) 747.
- [49] V.V. Anisovich and V.A. Nikonov, Eur. Phys. J. A8, 401 (2000); hep-ph/0008163 (2000).
- [50] V.V. Anisovich, UFN **174**, 49 (2004) [Physics-Uspekhi **47**, 45 (2004)].
- [51] G.F. Chew, *The analytic S-matrix*, NY, Benjamin, 1966.
- [52] A.V. Vereshagin, V.V. Vereshagin, Phys. Rev. **D58**:016002 (1999).
- [53] S. Pislak et al., Phys. Rev. Lett. **87**, 221801 (2001).
- [54] J.L. Basdevant, C.D. Frogatt and J.L. Petersen, Phys. Lett. **B41**, 178 (1972).
- [55] J.L. Basdevant and J. Zinn-Justin, Phys. Rev. **D3**, 1865 (1971); D. Iagolnitzer, J. Justin and J.B. Zuber, Nucl. Phys. **B60**, 233 (1973).
- [56] B.S. Zou and D.V. Bugg, Phys. Rev. **D48**, R3942 (1994); **D50**, 591 (1994).
- [57] G. Janssen, B.C. Pearce, K. Holinde and J. Speth, Phys. Rev. **D52**, 2690 (1995).
- [58] V.V. Anisovich, L.G. Dakhno, V.A. Nikonov, V.N. Markov, A.V. Sarantsev, Yad. Fiz. in press; hep-ph/0410361.
- [59] G.S. Bali et al., Phys. Lett. B **309** 378 (1993); J. Sexton, A. Vaccarino, and D. Weingarten, Phys. Rev. Lett. **75** 4563 (1995); C.J. Morningstar, M. Peardon, Phys. Rev. D **56** 4043 (1997).
- [60] L. Faddeev, A.J. Niemi and U. Wiedner, hep-ph/0308240 (2003).
- [61] D.V. Bugg, Phys. Rep., **397**, 257 (2004).





b



C

